Materials and Design 42 (2012) 505–512

Contents lists available at SciVerse ScienceDirect

Materials and Design

journal homepage: www.elsevier.com/locate/matdes

Microstructural characteristics and mechanical properties of non-combustive Mg–9Al–Zn–Ca magnesium alloy friction stir welded joints

L. Zhou [a,b,*], K. Nakata [a], J. Liao [c], T. Tsumura [a]

[a] Joining and Welding Research Institute, Osaka University, 11-1 Mihogaoka, Ibaraki, Osaka 567-0047, Japan
[b] Shandong Provincial Key Laboratory of Special Welding Technology, Harbin Institute of Technology at Weihai, Weihai 264209, China
[c] Technology Development Headquarters, Kurimoto Ltd., Osaka 559-0021, Japan

ARTICLE INFO

Article history:
Received 23 April 2012
Accepted 4 June 2012
Available online 15 June 2012

Keywords:
Friction stir welding
Non-combustive magnesium alloy
Microstructural characteristics
Mechanical properties

ABSTRACT

Non-combustive Mg–9Al–Zn–Ca magnesium alloy was friction stir welded with rotation speeds ranging from 500 to 1250 rpm at a constant welding speed of 200 mm/min. Defect-free joints were successfully produced at rotation speeds of 750 and 1000 rpm. The as-received hot extruded material consisted of equiaxed α-Mg grains with β-$Mg_{17}Al_{12}$ and Al_2Ca compounds distributed along the grain boundaries. Friction stir welding produced much refined α-Mg grains accompanied by the dissolution of the eutectic β-$Mg_{17}Al_{12}$ phase, while Al_2Ca phase was dispersed homogeneously into the Mg matrix. An increase in rotation speed increased the α-Mg grain size but not significantly, while microstructure in the heat affected zone was almost not changed compared with the base material. The hardness tests showed uniform distributed and slightly increased harness in the stir zone. Results of transverse tensile tests indicated that the defect-free joints fractured at the base material, while longitudinal tensile tests showed that the strength of the defect-free welds was improved due to microstructural refinement and uniform distribution of intermetallic compounds.

1. Introduction

Magnesium alloys are potential candidates to replace aluminum alloys in many structural applications owing to some of their unique properties of low density, high strength/weight ratio and so on. They are also considered as advanced materials in terms of electromagnetic shielding, energy conservation and environmental pollution regulation. In a wide range of the industries such as automotive, electronics and aerospace, magnesium alloys are increasingly widely used and expected to become one of the most promising lightweight materials in the 21st century [1]. However, oxidation and combustion of magnesium alloys in the melting, forging and heat treatment process obstruct their application greatly. Fortunately, there have been enormous efforts in developing non-combustive magnesium alloys in recent years. Alloying method by adding elements such as alkaline [2,3], rare earth [4–6] and their combination [7] to magnesium alloys to improve oxidation and combustion resistance is of great research and application prospect. For the non-combustive magnesium alloys developed so far, the Mg–Al–Zn–Ca system is promising for industrial applications due to satisfactory comprehensive properties and relatively low cost [8–14].

In order to apply magnesium alloys to structures, on the other hand, welding or joining technology is indispensable. Magnesium alloys are currently welded by almost all conventional fusion welding processes including gas tungsten arc welding (GTAW), gas metal arc welding (GMAW), plasma arc welding (PAW), electron beam welding (EBW) and laser beam welding (LBW). In recent years, some new processes like arc welding-bonding, laser welding-bonding and laser-arc hybrid welding are proposed for magnesium alloys. However, fusion welding technologies resulted in the formation of porosity, coarse microstructure, severe deformation and high residual stress in the joints. Brazing is also applied to magnesium alloys, but the joints are with low strength and poor heat resistance. Therefore, solid-state joining processes would appear to be more suitable for avoiding the problems associated with the melting of materials to be welded. Friction welding (FW) is used to achieve high performance joints of magnesium alloys, but it is limited because of the requirement for special geometric specifications and weld flash removal.

Friction stir welding (FSW) is a novel solid-state joining process invented by The Welding Institute (TWI) [15]. It can avoid many problems associated with conventional fusion welding processes, thereby producing defect-free welds with excellent properties, even in some materials with poor fusion-weldability. Compared with conventional friction welding process, this technology is versatile for workpiece geometry and the annoying flash removal

* Corresponding author. Tel.: +81 6 6879 8668; fax: +81 6 6879 8658.
E-mail address: zhouli@hitwh.edu.cn (L. Zhou).

0261-3069/$ - see front matter © 2012 Elsevier Ltd. All rights reserved.
http://dx.doi.org/10.1016/j.matdes.2012.06.005

process can be avoided. Due to its many advantages, FSW attracts a great deal of attention in the industrial world and has been successfully applied to the joining of various aluminum, magnesium and copper alloys. In recent years, FSW of high melting temperature materials such as steels, nickel and Ti alloys has become a research hotspot [16–18]. Though FSW of conventional magnesium alloys has been intensively investigated, especially for the Mg–Al–Zn (AZ) series [19–23], few studies dedicated to non-combustive magnesium alloys have been reported [24–27]. Zhang et al. [24] studied microstructural evolution of the non-combustive Mg–6%Al–3%Ca–0.5%R.E.–0.2%Mn magnesium alloy due to friction stir welding. Yamamoto et al. [25] and Chen et al. [26] conducted friction stir spot welding and friction stir welding of non-combustive Mg–6%Al–0.5%Mn–2% Ca (AMX602) magnesium alloy, respectively. Choi et al. [27] made microstructure evaluation of friction stir welded AZ91 with CaO non-combustive Mg Alloy. Until now, there has been no report about FSW of the non-combustive Mg–Al–Zn–Ca magnesium alloys. In the present study, the Mg–9Al–Zn–Ca magnesium alloy, denoted as AZX911, is friction stir welded, and microstructural characteristics and mechanical properties of the friction stir welded joints are investigated.

2. Experimental details

The as-received material was $300 \times 75 \times 4\ mm^3$ AZX911 plate hot extruded from starting ingot with the nominal chemical composition of Al 9.00, Zn 1.00, Ca 1.00 and Mg balance (all in wt.%). The plates were butt-welded together along the extrusion direction using a load-controlled type FSW equipment, as illustrated in Fig. 1. The rotating tool for FSW was made from tool steel consisted of a concave shoulder of 15 mm in diameter and a cylindrical pin with right-hand threads of 3.9 mm in length and 5 mm in diameter. The rotation speed was varied from 500 to 1250 rpm and the welding speed was kept constant at 200 mm/min. During the FSW, a 3° tilt and an applied force of 14 kN were applied to the FSW tool.

The welds were examined by X-ray radiography and metallurgical inspections were performed on the cross-section of the joints. The transverse joint cross-sections were cut by electrical discharge machining and prepared by standard metallographic procedure. The polished weld cross-sections were chemically etched using a solution of 10 g picric acid, 175 mL ethanol, 25 mL acetic acid, and 25 mL distilled water. The microstructures were observed by a Keyence VHX-200/100F optical microscope (OM) and a Hitachi SU-70 scanning electron microscope (SEM) equipped with an energy dispersive spectrometer (EDS). As shown in Fig. 1, BM, HAZ, TMAZ, and SZ in the joint cross-section stand for the base material, the heat affected zone, the thermomechanically affected zone and the stir zone, respectively. The advancing side is marked "AS" and the retreating side as "RS".

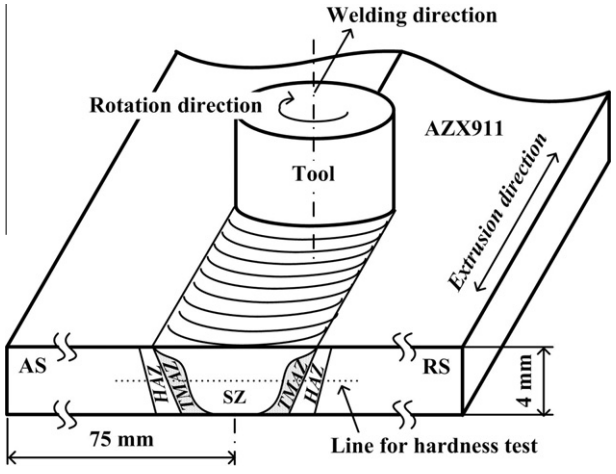

Fig. 1. Schematic illustration for friction stir welding.

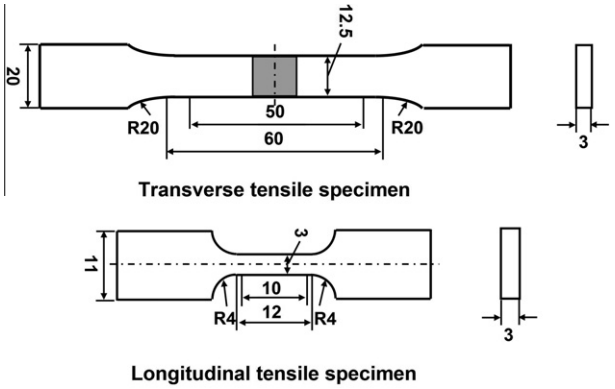

Fig. 2. Schematic illustration for dimension of transverse and longitudinal tensile specimen.

Vickers hardness along the transverse weld centerline was measured every 1 mm spacing on an Akashi AAV-500 Vickers hardness tester using a load of 0.49 N for 15 s. Transverse and longitudinal tensile test samples with geometric details shown in Fig. 2, were cut perpendicularly to the welding direction from the joint and parallel to the welding direction from the SZ, respectively, with the top and bottom surfaces eliminated. The configuration and size of the transverse tensile specimens were prepared according to JIS Z2201 [28], while small pieces were used for the longitudinal tensile test due to limitation of the weld geometry. Tensile tests were carried out on an Instron-5500 mechanical tester at room temperature using a crosshead speed of 0.2 mm/min. Furthermore, the facture surface after the tensile test was examined by SEM.

3. Results and discussion

3.1. Joint appearance

Joints with preferable surface appearance are obtained at rotation speeds of 500 and 750 rpm under the welding speed of 200 mm/min, as shown in Fig. 3. However, flash appears at the retreating side of the joints obtained at higher rotation speed due to increasing heat input, and it becomes more serious with increasing rotation speed. No obvious defects are observed on the X-ray radiography images for the joints obtained under rotation speed ranging from 500 to 1000 rpm. As for the 1250 rpm joint, there exist some internal defects indicated by red arrow at the advancing side.

The joints are further evaluated by cross-section check. It is shown that the 750 and 1000 rpm joints are defect-free, which is consistent with the radiographic examination. However, tiny flaws caused by insufficient heat input and thus plastic flow, which can not be detected by X-ray radiography, appear at the bottom of 500 rpm joint cross-section. As for the 1250 rpm joint, internal cavity defects are found at the advancing side. Generally, a large mass of flash appears in friction stir welded joints due to the excess heat input at higher rotation speed. However, cavity caused by the abnormal stirring would be formed under improper combination of high rotation speed and welding speed [29], which is just the case for the joint obtained at 1250 rpm.

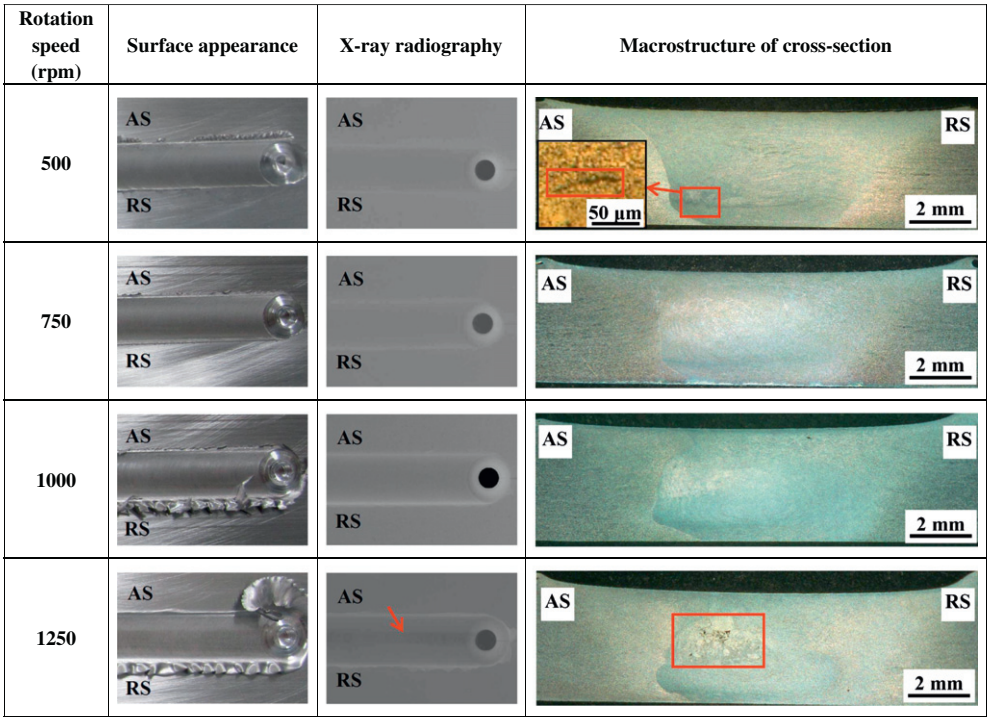

Fig. 3. Surface appearances and cross-sectional macrostructures of friction stir welded joints of hot extruded AZX911 magnesium alloy at various rotation speeds.

3.2. Microstructures in friction stir welded joint

Fig. 4 shows OM microstructures at different zones in the cross-section of typical joint welded with rotation speed of 500 rpm and welding speed of 200 mm/min. The BM exhibits a typical hot deformation structure formed in the extrusion process, having an equiaxed microstructure with α-Mg matrix and precipitated phase. Compared with the BM, microstructure in the HAZ is almost not changed. Grains in the TMAZ have been deformed and refined greatly due to the heat effect and mechanical deformation, and the grains have certain orientation along the metal-flow direction induced by stirring. The SZ contains a fine recrystallized microstructure, and the precipitated phase seems to be uniformly dispersed in the SZ.

With higher magnification image by SEM, a typical hot extruded microstructure is observed in the as-received AZX911 magnesium alloy, which is characterized by equiaxed primary α-Mg matrix and intermetallic compounds at the grain boundaries, as shown in Fig. 5. For the Mg–Al–Zn magnesium alloys with a high Al content, β-$Mg_{17}Al_{12}$ phase will be formed by a eutectic reaction

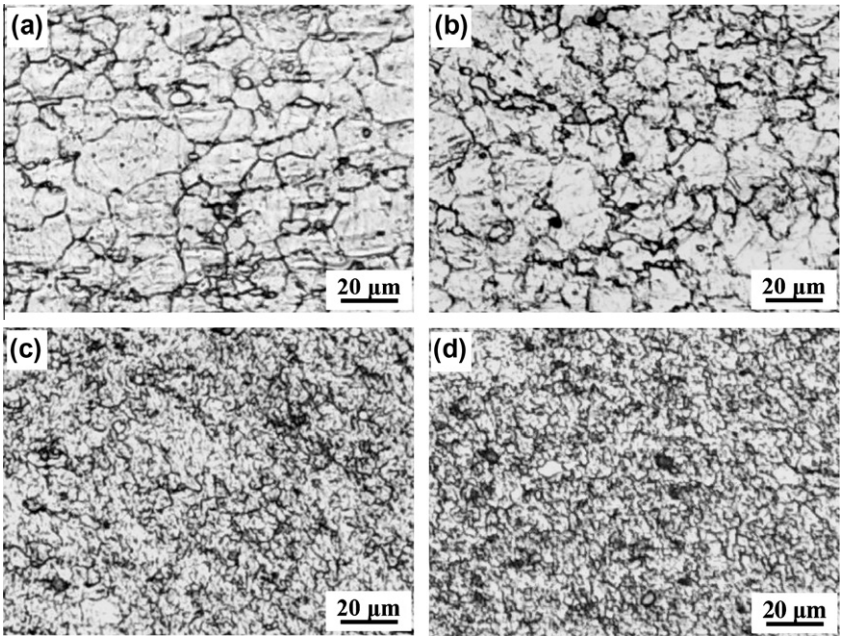

Fig. 4. OM micrographs of: (a) BM, (b) HAZ, (c) TMAZ and (d) SZ in the 500 rpm joint.

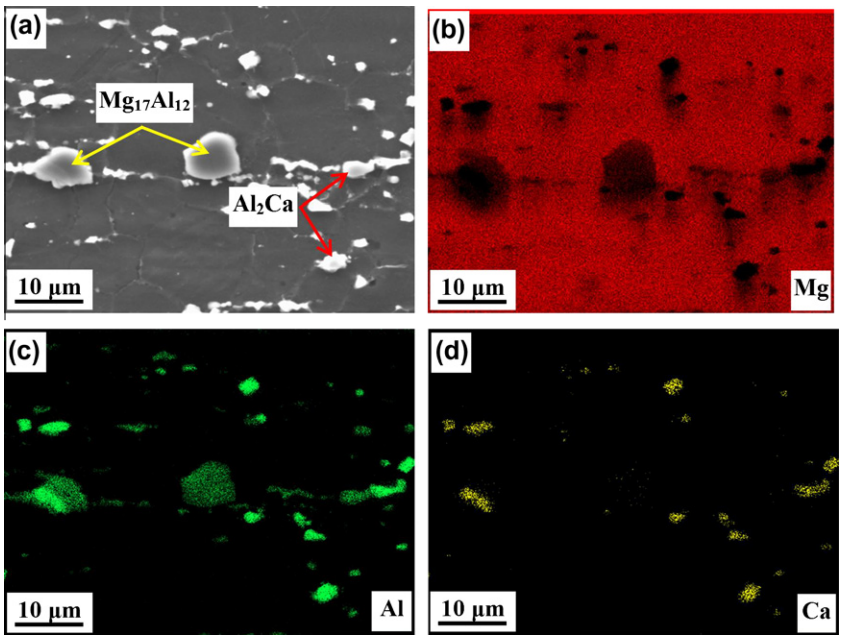

Fig. 5. EDS mapping of BM: (a) SEM micrograph, (b) Mg, (c) Al and (d) Ca.

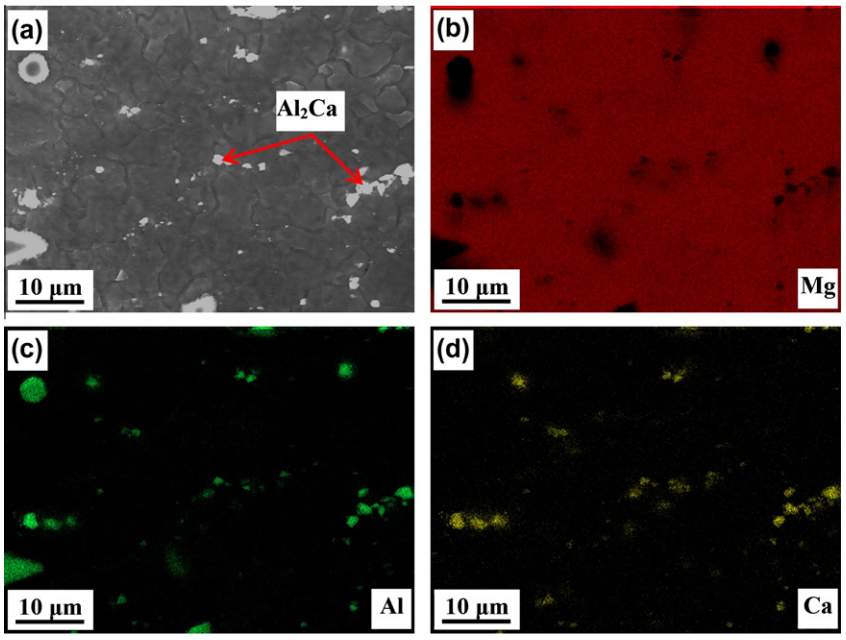

Fig. 6. EDS mapping of SZ in the 500 rpm joint: (a) SEM micrograph, (b) Mg, (c) Al and (d) Ca.

(L → α-Mg + β-$Mg_{17}Al_{12}$) during the non-equilibrium solidification [30]. However, the introduction of Ca to Mg-Al-Zn magnesium alloys will reduce the quantity of eutectic β-$Mg_{17}Al_{12}$ phase, and form new Al_2Ca phase [8,9]. As for the hot-extruded AZX911 magnesium alloy used in the present study, EDS mapping indicates coarse eutectic β-$Mg_{17}Al_{12}$ phase and relatively fine Al_2Ca phase formed due to Ca addition exist in the BM, which is consistent with the related studies.

Compared with the BM, the SZ consists of fine dynamically recrystallized equiaxed α-Mg grains and dispersed intermetallic compounds on SEM image, as shown in Fig. 6. However, EDS mapping of the SZ shows the coarse eutectic β-$Mg_{17}Al_{12}$ phase is dissolved into the α-Mg matrix, but the Al_2Ca phase remains. The eutectic β-$Mg_{17}Al_{12}$ phase is of poor thermal stability and will dissolve into the α-Mg matrix at temperature higher than 370 °C [30], which means the temperature of the SZ is over 370 °C during the welding process. However, the heating temperature does not exceed the solidus temperature, 500 °C, of the alloys because no cast microstructure was observed. As for the Al_2Ca phase with high thermal stability, the dissolution point is about 545 °C, which

exceeds the solidus temperature and much higher than that of the β-$Mg_{17}Al_{12}$ phase [14], and thus it will be retained but dispersed due to stirring.

3.3. Effect of rotation speed on microstructural evolution

TMAZ, where both the thermal and the plastic deformation effect are received, experiences partially recrystallization during the welding, and the microstructure is dependent on process parameters. High magnification SEM images of the TMAZ show there exist equiaxed dynamically recrystallized grains as well as elongated deformed grains, as shown in Fig. 7. The intermetallic phase has obvious orientation in TMAZ, and some of them have been fractured to smaller particles due to the mechanical deformation caused by stirring. Different from the SZ, coarse eutectic β-$Mg_{17}Al_{12}$ phase may remain in the TMAZ due to the inhomogeneous temperature distribution across the joint during the welding, and similar results have also been reported by Lee et al. [31]. With increasing rotation speed, the size of α-Mg matrix increases and the coarse eutectic β-$Mg_{17}Al_{12}$ phase decreases or even disappears through dissolution due to increasing heat input and thus temperature in the TMAZ.

The SEM microstructures in SZ welded at various rotation speeds with a constant welding speed of 200 mm/min are shown

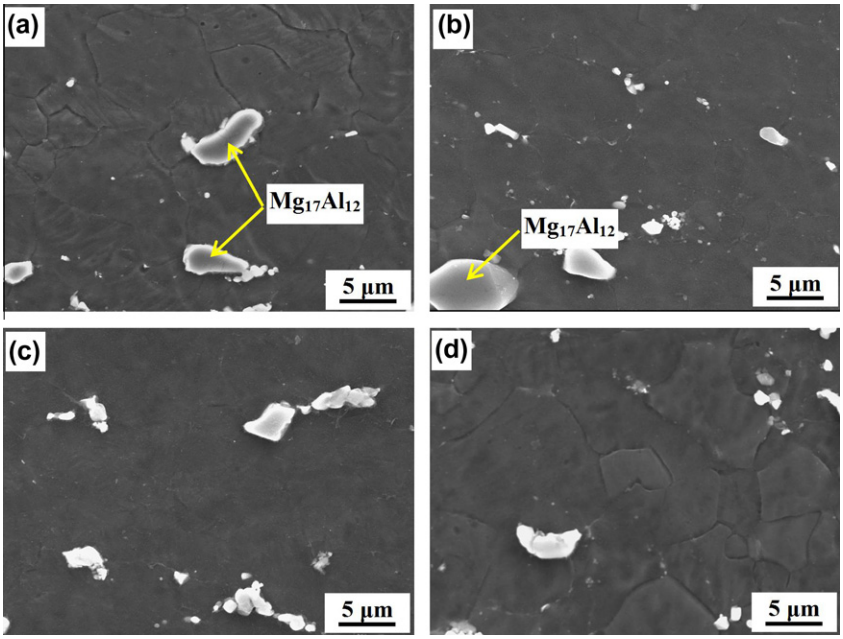

Fig. 7. Effect of rotation speed on SEM microstructure in the TMAZ of: (a) 500 rpm, (b) 750 rpm, (c) 1000 rpm and (d) 1250 rpm joint.

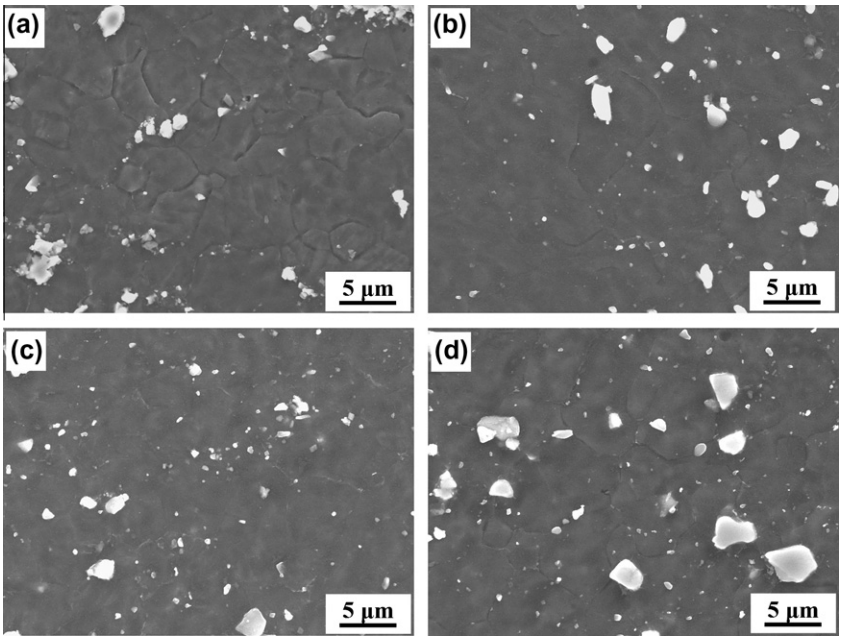

Fig. 8. Effect of rotation speed on SEM microstructure in the SZ of: (a) 500 rpm, (b) 750 rpm, (c) 1000 rpm and (d) 1250 rpm joint.

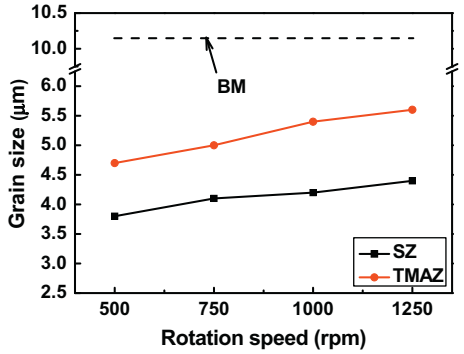

Fig. 9. Effect of rotation speed on grain size in TMAZ and SZ.

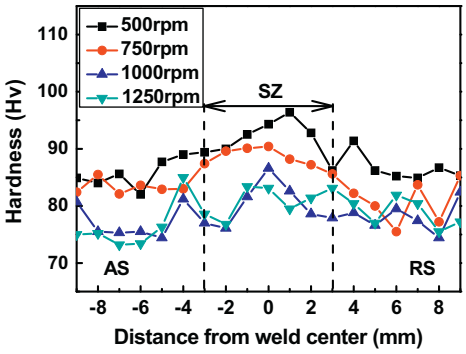

Fig. 10. Hardness distribution across the joints produced at different rotation speeds.

in Fig. 8. The microstructures in SZ obtained at various rotation speeds indicate recrystallized structure in SZ changes with welding conditions. At lower rotation speed, the α-Mg matrix is finer but the intermetallic compounds tend to aggregate at the grain boundaries as that in the BM. With increasing rotation speed, the size of α-Mg matrix increases due to increasing heat input, but the intermetallic compounds are more dispersed and homogeneously distributed in the matrix, which can be attributed to more obvious mechanical deformation effect in the SZ at higher rotation speed.

Grain size statistics show FSW produced much finer microstructure in the TMAZ and SZ compared with that in the BM, and grain size in the SZ is even finer than that in the TMAZ, which could be explained by recrystallization refinement and the recrystallization process is more significant in the SZ due to more significant mechanical deformation, as shown in Fig. 9. In addition, grain size in the TMAZ and SZ increases with increasing rotation speed due to increasing heat input. However, the effect of rotation speed on grain size is not so obvious, which probably can be attributed to that the dispersed Al_2Ca particles suppress grain growth via Zener pinning of the grain boundaries, and finally fine grains are formed even at high rotation speeds [32].

3.4. Hardness profile across the joints

Vickers hardness distribution across the joints is shown in Fig. 10. The BM has a very wide range of hardness, which is measured approximately from 70 to 85 Hv. The BM is composed of α-Mg matrix and precipitated intermetallic compounds. The α-Mg phase, which is softer than the intermetallic phase, has a large volume fraction. If the measured hardness indenter were located near primary α-Mg phase than precipitated phase, the hardness

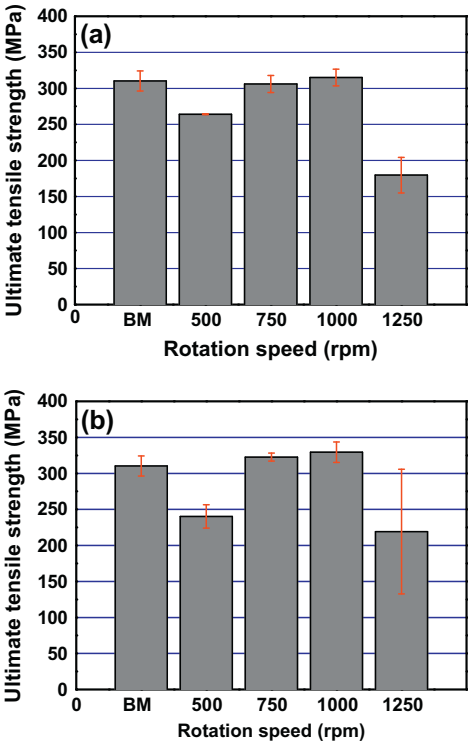

Fig. 11. Effect of rotation speed on: (a) transverse tensile properties and (b) longitudinal tensile properties.

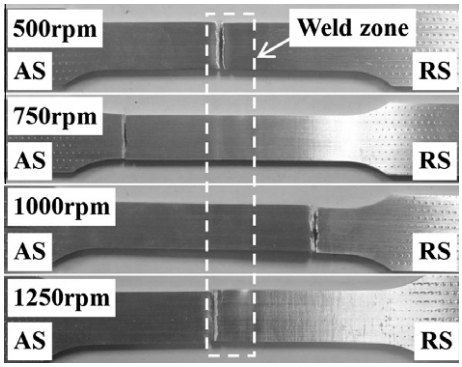

Fig. 12. Fracture location of the transverse tensile specimens for: (a) 500 rpm, (b) 750 rpm, (c) 1000 rpm and (d) 1250 rpm joint.

shows relatively low value of about 70 Hv. However, in the opposite situation, the hardness of the BM shows about 85 Hv. Compared with the BM, the hardness tests showed uniform distributed and slightly increased harness in the SZ, and the hardness value decreases with increasing rotation speed but not significantly. No obvious hardness difference between the AS and RS is observed because there is no obvious microstructure difference between the AS and RS.

The dissolution of β-$Mg_{17}Al_{12}$ phase into α-Mg matrix will lower hardness in the alloy, but the homogenous recrystallization refinement of α-Mg matrix and dispersed distribution of Al_2Ca phase result in uniform distribution and slight increase of hardness in the SZ. Furthermore, the average grain size has a great influence on hardness in the friction stir weld according to the Hall–Petch relation. As for the as-received AZX911 magnesium alloy, grain size in the SZ increases with increasing rotation speed but not

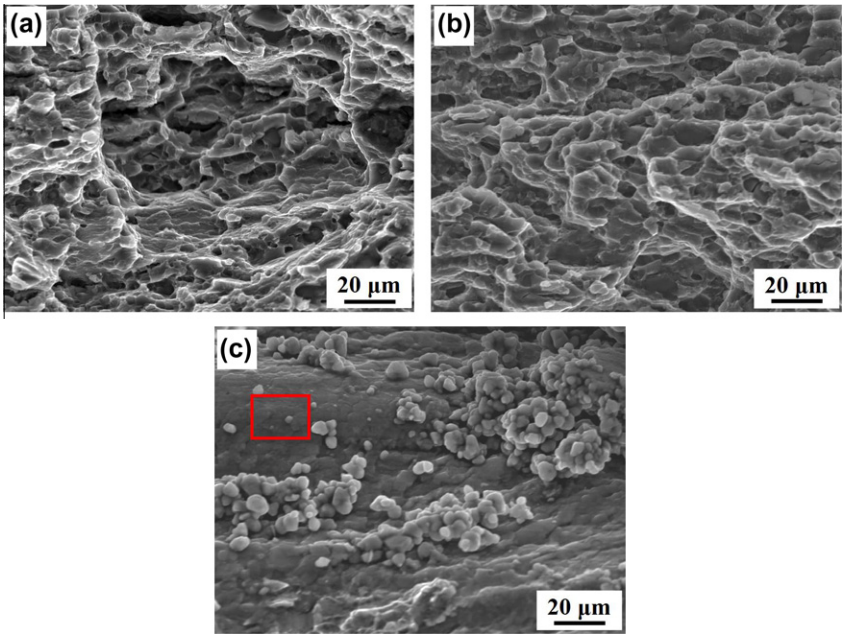

Fig. 13. Fracture surface morphology of transverse tensile specimens for: (a) BM/750 and 1000 rpm, (b) 500 rpm and (c) 1250 rpm joint.

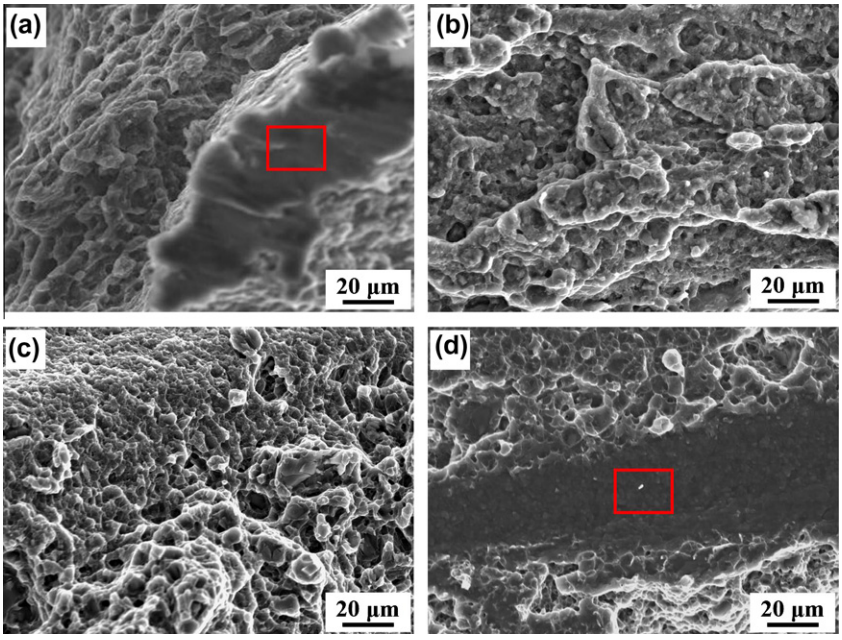

Fig. 14. Fracture surface morphology of longitudinal tensile specimens for: (a) 500 rpm, (b) 750 rpm, (c) 1000 rpm and (d) 1250 rpm joint.

obviously, which gives explanation for hardness in the SZ decreases with increasing rotation speed but not significantly.

3.5. Transverse and longitudinal tensile test

Tensile test results and fracture location of the joints are summarized in Figs. 11 and 12, respectively. The defect-free joints fracture at the BM and the tensile strength is equivalent to that of the BM, while the joints with defects fracture at the advancing side, where the defects are formed, and the tensile strength is much lower than that of the BM. However, longitudinal tensile tests show the tensile strength of the defect-free joints is improved, and there is little difference between the joints obtained at 750 and 1000 rpm.

Many studies have demonstrated that a friction stir welded joint having heterogeneous hardness distribution fails in the minimum hardness region, and the tensile property of the defect-free joint is dependent on the minimum hardness region in the entire joint [33,34]. As for the defected joints, it is certainly that the fracture occurs at the location of defects during transverse or longitudinal tensile test despite of the hardness distribution, and the tensile strength is much lower than that of the BM. The defect-free transverse tensile specimens fracture at minimum hardness region, the BM, and thus the tensile strength is equivalent to that

of the BM, as shown in Fig. 11a. For metallic materials, the strength is generally proportional to the hardness, and thus tensile strength of the defect-free longitudinal specimens cut from the SZ is higher than that of the BM due to the increase of hardness induced by microstructural refinement and dispersed distribution of intermetallic compounds. In addition, there is little difference in hardness of the SZ obtained at 750 and 1000 rpm, therefore the longitudinal tensile strength is almost the same, as indicated by Fig. 11b.

The fracture surfaces of the transverse and longitudinal tensile specimens are shown in Figs. 13 and 14, respectively. The fracture surface morphology of BM and defect-free joints shows plastic fracture characterized by dimples. In addition, the fracture surface of defect-free joints exhibits small dimples, which are probably resulted from the homogeneous microstructure of fine grains. As for the defected joints, the fracture surface presents brittle rupture characteristics at the defective areas, as indicated by red frame. As for the 500 rpm joint with a tiny defect (see Fig. 3), it should be noted that the tensile force is parallel to the defect during the transverse tensile test, and thus no obvious brittle rupture area is observed on the fracture surface (see Fig. 13b). However, the tensile force is vertical to the defect during longitudinal tensile test and obvious brittle rupture area is formed (see Fig. 14a). It can be concluded from the above results that FSW is a very useful modification method for the mechanical property improvement of non-combustive Mg–9Al–Zn–Ca magnesium alloy, because it refines and uniforms the microstructure and intermetallic compounds.

4. Conclusions

In the present study, hot extruded non-combustive Mg–9Al–Zn–Ca magnesium alloy is friction stir welded with rotation speeds ranging from 500 to 1250 rpm at a constant welding speed of 200 mm/min, and microstructural characteristics and mechanical properties of friction stir welded joints are investigated. Defect-free joints are obtained under tool rotation speed of 750 and 1000 rpm. At the rotation speed of 500 and 1250 rpm, a tiny defect and abnormal stirring induced cavity-defect due to insufficient or excessive heat input and plastic flow are formed, respectively. The as-received material consists of equiaxed α-Mg grains with β-$Mg_{17}Al_{12}$ and Al_2Ca compounds distributed along the grain boundaries. Friction stir welding produces much refined α-Mg grains accompanied by the dissolution of the eutectic β-$Mg_{17}Al_{12}$ phase, while Al_2Ca phase is dispersed homogeneously into the matrix. An increase in rotation speed increases the α-Mg grain size but not significantly, while microstructure in the heat affected zone is almost not changed compared with that in the base material. The hardness tests show uniform distributed and increased harness in the stir zone. The defect-free joints fracture at the base material during transverse tensile test, while longitudinal tensile tests show that the strength of the defect-free welds is improved due to microstructural refinement and dispersed distribution of intermetallic compounds.

References

[1] Polmear IJ. Magnesium alloys and applications. Mater Sci Technol 1994;10:1–16.
[2] Sakamoto M, Akiyama S. Suppression of ignition and burning of molten Mg alloys by Ca bearing stable oxide film. J Mater Sci Lett 1997;16:1048–50.
[3] Shih TS, Wang JH, Chong KZ. Combustion of magnesium alloys in air. Mater Chem Phys 2004;85:302–9.
[4] Ravi Kumar NV, Blandin JJ, Suery M, Grosjean E. Effect of alloying elements on the ignition resistance of magnesium alloys. Scr Mater 2003;49:225–30.
[5] Fan JF, Yang GC, Chen SL, Xie H, Wang M, Zhou YH. Effect of rare earths (Y, Ce) additions on the ignition points of magnesium alloys. J Mater Sci 2004;39:6375–7.
[6] Fan JF, Yang CL, Han G, Fang S, Yang WD, Xu BS. Oxidation behavior of ignition-proof magnesium alloys with rare earth addition. J Alloy Compd 2011;509:2137–42.
[7] Zeng XQ, Wang QD, Lu YZ, Ding WJ, Lu C, Zhu YP, et al. Study on ignition proof magnesium alloy with beryllium and rare earth additions. Scr Mater 2000;43:403–9.
[8] Wang QD, Chen WZ, Zeng XQ, LU YZ, Ding WJ, Zhu YP, et al. Effects of Ca addition on the microstructure and mechanical properties of AZ91 magnesium alloy. J Mater Sci 2001;36:3035–40.
[9] Li SS, Tang B, Zeng DB. Effects and mechanism of Ca on refinement of AZ91D alloy. J Alloy Compd 2007;437:317–21.
[10] Hakamada M, Watazu A, Saito N, Iwasaki H. Tensile properties of forged Mg–Al–Zn–Ca alloy. Mater Trans 2008;49:554–8.
[11] Park J, Kim M, Yoon U, Kim W. Microstructures and mechanical properties of Mg–Al–Zn–Ca alloys fabricated by high frequency electromagnetic casting method. J Mater Sci 2009;44:47–54.
[12] Hakamada M, Shimizu K, Yamashita T, Watazu A, Saito N, Iwasaki H. Effect of initial microstructures on hot forging of Ca-containing cast Mg alloys. J Mater Sci 2010;45:719–24.
[13] Hakamada M, Watazu A, Saito N, Iwasaki H. Dynamic recrystallization during hot compression of as-cast and homogenized noncombustible Mg–9Al–1Zn–1Ca (in mass%) alloys. Mater Sci Eng A 2010;527:7143–6.
[14] Xu SW, Kamado S, Honma T. Recrystallization mechanism and the relationship between grain size and Zener–Hollomon parameter of Mg–Al–Zn–Ca alloys during hot compression. Scr Mater 2010;63:293–6.
[15] Thomas WM, Nicholas ED, NeedHam JC, Murch MG, Templesmith P, Dawes CJ. Friction stir welding. International patent application no. PCT/GB92102203 and Great Britain patent application no. 9125978. 8; 1991.
[16] Mishra RS, Ma ZY. Friction stir welding and processing. Mater Sci Eng R 2005;50:1–78.
[17] Nandan R, DebRoy T, Bhadeshia H. Recent advances in friction stir welding – process, weldment structure and properties. Prog Mater Sci 2008;53:980–1023.
[18] Threadgill PL, Leonard AJ, Shercliff HR, Withers PJ. Friction stir welding of aluminium alloys. Int Mater Rev 2009;54:49–93.
[19] Cao X, Jahazi M. Effect of welding speed on the quality of friction stir welded butt joints of a magnesium alloy. Mater Des 2009;30:2033–42.
[20] Forcellese A, Gabrielli F, Simoncini M. Mechanical properties and microstructure of joints in AZ31 thin sheets obtained by friction stir welding using "pin" and "pinless" tool configurations. Mater Des 2012;34:219–29.
[21] Forcellese A, Simoncini M. Plastic flow behaviour and formability of friction stir welded joints in AZ31 thin sheets obtained using the "pinless" tool configuration. Mater Des 2012;36:123–9.
[22] Liu D, Nishio H, Nakata K. Anisotropic property of material arrangement in friction stir welding of dissimilar Mg alloys. Mater Des 2011;32:4818–24.
[23] Zhang H, Lin SB, Wu L, Feng JC, Ma SL. Defects formation procedure and mathematic model for defect free friction stir welding of magnesium alloy. Mater Des 2006;27:805–9.
[24] Zhang DT, Suzuki M, Maruyama K. Microstructural evolution of a heat-resistant magnesium alloy due to friction stir welding. Scr Mater 2005;52:899–903.
[25] Yamamoto N, Liao JS, Nakata K. Friction stir weldability of high tensile strength Mg–Zn–Al–Ca–La magnesium alloy consisted of fine grain. J Jpn Inst Met 2008;72:538–43.
[26] Chen J, Fujii H, Sun YF, Morisada Y, Kondoh K, Hashimoto K. Effect of grain size on the microstructure and mechanical properties of friction stir welded non-combustive magnesium alloys. Mater Sci Eng A 2012. http://dx.doi.org/10.1016/j.msea.2012.04.03.
[27] Choi DH, Ahn BW, Kim SK, Yeon YM, Kim YJ, Park SK, et al. Microstructure evaluation of friction stir welded AZ91 with CaO Mg alloy. Mater Trans 2011;52:802–5.
[28] Japanese Standards Association. Tensile pieces for tensile test for metallic materials. Japanese industrial standard: JIS Z2201; 2004.
[29] Kim YG, Fujii H, Tsumura T, Komazaki T, Nakata K. Three defect types in friction stir welding of aluminum die casting alloy. Mater Sci Eng A 2006;415:250–4.
[30] Massalski TB. Binary alloy phase diagram, vol. 1. Ohio: ASM International; 1986.
[31] Lee WB, Kim JW, Yeon YM, Jung SB. The joint characteristics of friction stir welded AZ91D magnesium alloy. Mater Trans 2003;44:917–23.
[32] Liao JS, Yamamoto N, Nakata K. Effect of dispersed intermetallic particles on microstructural evolution in the friction stir weld of a fine-grained magnesium alloy. Metall Mater Trans A 2009;40:2212–9.
[33] Liu HJ, Fujii H, Maeda M, Nogi K. Mechanical properties of friction stir welded joints of 1050–H24 aluminium alloy. Sci Technol Weld Join 2003;8:450–4.
[34] Ren SR, Ma ZY, Chen LQ. Effect of welding parameters on tensile properties and fracture behavior of friction stir welded Al–Mg–Si alloy. Scr Mater 2007;56:69–72.